

Robust Least-Squares Optimization for Data-Driven Predictive Control: A Geometric Approach

Shreyas Bharadwaj

Indian Institute of Technology Bombay, India

SHREYASNB@IITB.AC.IN

Bamdev Mishra

Microsoft India

BAMDEVM@MICROSOFT.COM

Cyrus Mostajeran

Nanyang Technological University, Singapore

CYRUSSAM.MOSTAJERAN@NTU.EDU.SG

Alberto Padoan

University of British Columbia, Vancouver, Canada

APADOAN@ECE.UBC.CA

Jeremy Coulson

University of Wisconsin-Madison, USA

JEREMY.COULSON@WISC.EDU

Ravi N Banavar

Indian Institute of Technology Bombay, India

BANAVAR@IITB.AC.IN

Abstract

The paper studies a geometrically robust least-squares problem that extends classical and norm-based robust formulations. Rather than minimizing residual error for fixed or perturbed data, we interpret least-squares as enforcing approximate subspace inclusion between measured and true data spaces. The uncertainty in this geometric relation is modeled as a metric ball on the Grassmannian manifold, leading to a min–max problem over Euclidean and manifold variables. The inner maximization admits a closed-form solution, enabling an efficient algorithm with a transparent geometric interpretation. Applied to robust finite-horizon linear–quadratic tracking in data-enabled predictive control, the method improves upon existing robust least-squares formulations, achieving stronger robustness and favorable scaling under small uncertainty.

Keywords: least-squares, differential geometry, optimization, data-driven control

1. Introduction

Least-squares optimization is a ubiquitous problem in science and engineering. The problem is classically defined as

$$\min_{x \in \mathbb{R}^k} \|Ax - b\|_2^2,$$

where $A \in \mathbb{R}^{n \times k}$ and $b \in \mathbb{R}^n$ are given data, and $x \in \mathbb{R}^k$ is the decision variable. In regression problems, the matrix A represents a linear model and typically contains the regressors, while the vector b collects the measured responses. The objective penalizes the residual $Ax - b$ in the Euclidean norm, yielding the coefficient vector x that best fits the data in the least-squares sense. The origins of least-squares trace back to celestial mechanics (Gauss, 1809), and the method has since become indispensable across scientific and engineering disciplines. In control theory, least-squares formulations are ubiquitous and underpin tasks such as identification, filtering, and optimal control. Despite its broad applicability, the least-squares solution is well known to be sensitive to perturbations in the data, especially when A is ill-conditioned (Golub and Van Loan, 2013).

The *total least-squares* problem (Golub and Van Loan, 1980) generalizes classical least-squares by allowing perturbations in the individual matrix entries of both A and b . As in ordinary least-squares, the resulting solution may be sensitive to perturbations in the data (Golub and Van Loan, 2013). Sensitivity to perturbations in the data (A, b) can be mitigated in various ways. One strategy is to consider the *robust* least-squares problem

$$\min_{x \in \mathbb{R}^k} \max_{A \in \mathbb{B}_\rho(\hat{A})} \|Ax - b\|_2^2,$$

where $\mathbb{B}_\rho(\hat{A})$ is the metric ball of radius ρ centered at \hat{A} defined by a given metric. The specific choice of metric reflects the interpretation assigned to the data matrix, see, e.g., (El Ghaoui and Lebret, 1997), (Markovsky and Van Huffel, 2007).

In this paper, we consider a robust least-squares formulation that incorporates the *geometric* nature of perturbations in linear models. In particular, we consider

$$\min_{x \in \mathbb{R}^n} \max_{\mathcal{Y} \in \mathbb{B}_\rho^d(\hat{\mathcal{Y}})} \|P_{\mathcal{Y}}x - b\|_2^2, \quad (1)$$

where $P_{\mathcal{Y}}$ denotes the orthogonal projector onto a k -dimensional subspace \mathcal{Y} of \mathbb{R}^n , and $\mathbb{B}_\rho^d(\hat{\mathcal{Y}})$ is a ball of radius ρ around $\hat{\mathcal{Y}}$ in the Grassmannian $\text{Gr}(k, n)$, i.e., the manifold of k -dimensional subspaces of \mathbb{R}^n . The problem builds on the formulation introduced in (Coulson et al., 2025), and is motivated by a wide range of applications, including robust subspace tracking in signal processing (Delmas, 2010), computer vision (He et al., 2012), and system identification (Sasfi et al., 2024).

Our motivating application arises in data-driven predictive control (Coulson et al., 2019), where uncertainty fundamentally enters through the finite-horizon behavior of a linear time-invariant (LTI) system. In the behavioral approach (Willems et al., 2005), the finite-horizon trajectories of an LTI system form a finite-dimensional subspace and can be characterized as the image of a Hankel matrix constructed from data, by the *fundamental lemma* (Willems et al., 2005). Hence, a range of data-driven predictive control methods — in both deterministic (Coulson et al., 2019; De Persis and Tesi, 2019; Berberich et al., 2022) and stochastic settings (Breschi et al., 2023) — rely on dynamic constraints expressed as subspaces, which are naturally modeled as points on the *Grassmannian*. As a consequence, uncertainty in the data translates directly into subspace uncertainty. This perspective has proved effective in mode recognition, fault detection, and system identification (Padoan et al., 2022; Padoan and Coulson, 2025). In line with these findings, we show in Section 3 that (1) captures this geometric uncertainty while preserving favorable structure and providing robustness guarantees for data-driven predictive control.

Related work. Robust extensions of least-squares problem have been explored under various perturbation models, including norm-bounded uncertainty (El Ghaoui and Lebret, 1997), total least-squares (Golub and Van Loan, 1980), and geometric formulations on matrix manifolds (Absil et al., 2007), the latter being closest to the setting considered here. In this work, we build on (Coulson et al., 2025) and study a constrained variant of the geometric robust least-squares problem, which requires dedicated analysis due to the interaction between the constraints and the subspace uncertainty set. Robust formulations for model predictive control (MPC) trace back to the seminal work of (Mayne et al., 2005) and have been extensively studied for linear systems, including in data-driven settings (Scokaert and Mayne, 1998; Xie et al., 2024, 2025, 2026). Data-driven predictive control methods often rely on behavioral formulations in which feasible trajectories lie in a

data-determined subspace, both in deterministic (Coulson et al., 2019; De Persis and Tesi, 2019; Berberich et al., 2022) and in stochastic (Breschi et al., 2023) settings (see also Markovsky and Dörfler (2021) for an overview). Related developments include robust extensions of direct data-driven MPC (Huang et al., 2021), and unifying perspectives that connect direct (behavioral) and indirect (model-based) schemes via regularization and relaxation (Dörfler et al., 2023). Closest to our setting are (Xie et al., 2024, 2025, 2026), which also address min–max data–driven MPC. Their formulations rely on linear matrix inequalities (LMIs) and require knowledge of the system order and state dimensions. In contrast, our approach remains order–free, avoids explicit state parameterization, and yields a scalable alternative to LMI–based designs.

Contributions. The article presents a tractable and geometrically grounded formulation of the robust least-squares problem arising in data-driven predictive control. Building on the extended abstract (Coulson et al., 2025), uncertainty is modeled as a metric ball on the Grassmannian manifold, leading to a min–max optimization problem that captures geometric robustness in a principled way. Our main contribution, in contrast to (Coulson et al., 2025), is an analytic, closed-form solution to the inner maximization, which transforms the original nonconvex problem into a convex and computationally efficient formulation. The resulting algorithm constitutes a marked improvement over the algorithm introduced in (Coulson et al., 2025), offering significantly faster convergence and lower computational cost. This novel tractability allows us to apply the methodology to data-driven predictive control, where algorithm scalability is vital. Compared with data-driven MPC (Berberich et al., 2021), our method achieves similar tracking performance while providing a clear system-theoretic interpretation of robustness in terms of finite-horizon trajectories.

2. Preliminaries

The *Grassmannian* $\text{Gr}(k, n)$ is the Riemannian manifold of all k -dimensional linear subspaces of \mathbb{R}^n (Boumal, 2023). A standard way to describe it is through the *Stiefel manifold* $\text{St}(k, n) := \{ Y \in \mathbb{R}^{n \times k} : Y^\top Y = I_k \}$, whose elements are matrices with orthonormal columns. An alternative convenient representation uses orthogonal projection matrices. Every k -dimensional subspace \mathcal{Y} of \mathbb{R}^n admits a unique orthogonal projector $P_{\mathcal{Y}}$, which makes this identification natural. In this representation, the Grassmannian can be written as $\text{Gr}(k, n) = \{ P \in \mathbb{R}^{n \times n} : P^\top = P, P^2 = P, \text{rank}(P) = k \}$, where each point corresponds to a unique symmetric, idempotent matrix of rank k , and the associated k -dimensional subspace is given by the image of P . The link between these two representations is given by the canonical projection $\pi : \text{St}(k, n) \rightarrow \text{Gr}(k, n)$ such that $\pi(Y) = YY^\top$, which maps an orthonormal basis Y to the orthogonal projector onto its span. Given a smooth function $f : \text{Gr}(k, n) \rightarrow \mathbb{R}$, its Riemannian gradient at \mathcal{Y} is the orthogonal projector of the Euclidean gradient of any smooth extension $\bar{f} : \mathbb{R}^{n \times k} \rightarrow \mathbb{R}$ onto the tangent space:

$$\text{grad}f(\mathcal{Y}) = P_{\mathcal{Y}}^\perp \nabla \bar{f}(Y), \quad P_{\mathcal{Y}}^\perp := I_n - YY^\top,$$

where \bar{f} satisfies $\bar{f}(Y) = f(\mathcal{Y})$ for any orthonormal basis Y of \mathcal{Y} , and $\nabla \bar{f}(Y)$ denotes the standard Euclidean gradient of \bar{f} .

Several distances can be used to compare subspaces (Boumal, 2023), such as geodesic, projection, and Procrustes distances. The *chordal distance* is particularly convenient because it admits a simple expression in terms of projection matrices and is computationally efficient. It is defined as

$$d(\mathcal{Y}_1, \mathcal{Y}_2) := \sqrt{\text{Tr}(P_{\mathcal{Y}_1}^\perp P_{\mathcal{Y}_2})}. \quad (2)$$

2.1. Behaviors and data-driven representations of dynamical systems

Consider the discrete-time LTI state-space system

$$x(t+1) = Ax(t) + Bu(t), \quad y(t) = Cx(t) + Du(t), \quad (3)$$

where $u(t) \in \mathbb{R}^m$ is the input, $y(t) \in \mathbb{R}^p$ is the output, and $x(t) \in \mathbb{R}^n$ is the state for $t \in \mathbb{N}$. The input-output behavior (Willems, 1986) of the state-space system (3) is defined as

$$\mathfrak{B} := \{w = (u, y) : \mathbb{N} \rightarrow \mathbb{R}^{m+p} \mid \exists x : \mathbb{N} \rightarrow \mathbb{R}^n \text{ such that (3) holds for all } t \in \mathbb{N}\}. \quad (4)$$

Given \mathfrak{B} as above, we call (3) a state-space representation of \mathfrak{B} and elements of \mathfrak{B} *trajectories*. We assume without loss of generality that the state-space system (3) is *minimal*, in the sense that n is as small as possible across all state-space representations of \mathfrak{B} . The *lag* of \mathfrak{B} is defined as the smallest integer ℓ such that $\text{rank}[C^\top A^\top C^\top \cdots (A^{\ell-1})^\top C^\top]^\top = \text{rank}[C^\top A^\top C^\top \cdots (A^\ell)^\top C^\top]^\top$.

The restriction of a trajectory $w : \mathbb{N} \rightarrow \mathbb{R}^{m+p}$ to a nonempty interval $[i, j]$ is defined as $w|_{[i,j]} = \text{col}(w(i), w(i+1), \dots, w(j))$, where $\text{col}(w_1, \dots, w_k) := [w_1^\top \cdots w_k^\top]^\top$. The *restricted behavior* is defined as $\mathfrak{B}|_{[1,L]} := \{w|_{[1,L]} \mid w \in \mathfrak{B}\}$.

We define the *Hankel matrix* of depth $L \in \mathbb{N}$, associated with a vector $w|_{[1,T]} \in \mathbb{R}^{qT}$ as

$$\mathcal{H}_L(w|_{[1,T]}) = \begin{bmatrix} w(1) & w(2) & \cdots & w(T-L+1) \\ w(2) & w(3) & \cdots & w(T-L+2) \\ \vdots & \vdots & \ddots & \vdots \\ w(L) & w(L+1) & \cdots & w(T) \end{bmatrix}.$$

The restricted behavior of LTI system (3) is a subspace, whose dimension is determined only by its state-space dimension n , lag ℓ , and time horizon $[1, L]$.

Lemma 1 (Dörfler et al., 2023, Lemma 2.1) *Consider the LTI system (3) with associated behavior \mathfrak{B} . The restricted behavior $\mathfrak{B}|_{[1,L]}$ is a linear subspace of \mathbb{R}^{qL} . Moreover, for $L \geq \ell$, $\dim \mathfrak{B}|_{[1,L]} = mL + n$.*

As a direct consequence of Lemma 1, the restricted behavior can be represented as the image of a raw data matrix. A version of this result known as the *fundamental lemma* (Willems et al., 2005) is presented below.

Lemma 2 (Markovsky and Dörfler, 2023, Corollary 19) *Consider the LTI system (3) with associated behavior \mathfrak{B} . Let $L > \ell$, $T \geq L$, and $w|_{[1,T]} \in \mathfrak{B}|_{[1,T]}$. Then, $\mathfrak{B}|_{[1,L]} = \text{im } \mathcal{H}_L(w|_{[1,T]})$, if and only if $\text{rank } \mathcal{H}_L(w|_{[1,T]}) = mL + n$.*

This condition is referred to as the *generalized persistency of excitation* (GPE) condition.

2.2. Finite-horizon linear quadratic tracking

Given an LTI system, an initial trajectory compatible with its behavior, and a quadratic cost, the linear quadratic tracking problem is to find a trajectory that is as close as possible to a given reference. Over a finite-horizon, the problem can be formulated as follows (Markovsky and Rapisarda, 2008): Consider the system (3) with associated behavior \mathfrak{B} , an initial trajectory $w_{\text{ini}} \in \mathfrak{B}|_{[1,T_{\text{ini}}]}$,

with $T_{\text{ini}} \geq 1$, a reference $w_{\text{ref}} \in \mathbb{R}^{qT_f}$, with $T_f \geq 1$, and a symmetric positive definite matrix $\Phi \in \mathbb{R}^{q \times q}$. The *linear quadratic tracking (LQT) problem* is to find a trajectory w_f that minimizes the quadratic cost

$$\|w_f - w_{\text{ref}}\|_{I \otimes \Phi}^2 = \sum_{t=1}^{T_f} (w_f(t) - w_{\text{ref}}(t))^{\top} \Phi (w_f(t) - w_{\text{ref}}(t)),$$

and has a *past constraint* on the initial trajectory w_{ini} , i.e.,

$$\begin{aligned} \min_{w_f \in \mathbb{R}^{qT_f}} \quad & \|w_f - w_{\text{ref}}\|_{I \otimes \Phi}^2 \\ \text{subject to} \quad & \text{col}(w_{\text{ini}}, w_f) \in \mathfrak{B}|_{[1, T_{\text{ini}} + T_f]}. \end{aligned} \tag{5}$$

If a parametric model of the system behavior is available – for example, a state-space representation – (5) gives rise to a classical finite-horizon optimal control problem (Anderson and Moore, 1990).

3. Proposed Geometric Modeling

The finite-horizon LQT problem (5) admits a natural least-squares reformulation: the cost in (5) is quadratic, and the requirement that $\text{col}(w_{\text{ini}}, w_f) \in \mathfrak{B}|_{[1, T_{\text{ini}} + T_f]}$ is a subspace constraint. Consequently, identifying the restricted behavior $\mathfrak{B}|_{[1, T_{\text{ini}} + T_f]}$ with a subspace $\hat{\mathcal{Y}} \in \text{Gr}(k, n)$, any feasible trajectory $w \in \mathfrak{B}|_{[1, T_{\text{ini}} + T_f]}$ of problem (5) satisfies

$$w = P_{\hat{\mathcal{Y}}} x, \text{ for some } x \in \mathbb{R}^{qL},$$

where $L = T_{\text{ini}} + T_f$, along with the affine constraint enforcing consistency with the observed past,

$$Mw = w_{\text{ini}}, \quad \text{where } M := [I_{qT_{\text{ini}}} \ 0] \in \mathbb{R}^{qT_{\text{ini}} \times qL}.$$

Substituting these expressions in (5) shows that finite-horizon LQT reduces to a constrained least-squares problem

$$\min_{x \in \mathbb{R}^{qL}} \|P_{\hat{\mathcal{Y}}} x - b\|_2^2 \quad \text{s.t.} \quad MP_{\hat{\mathcal{Y}}} x = Mb, \tag{6}$$

where $b := \text{col}(w_{\text{ini}}, w_{\text{ref}})$.

In practice, the subspace $\hat{\mathcal{Y}}$ is estimated from finite, noisy data, motivating a robust formulation. Motivated and inspired by (Coulson et al., 2025), one may allow the behavior subspace to vary within a ball $\mathbb{B}_{\rho}^d(\hat{\mathcal{Y}})$, yielding

$$\begin{aligned} \min_{x \in \mathbb{R}^{qL}} \quad & \max_{\mathcal{Y} \in \mathbb{B}_{\rho}^d(\hat{\mathcal{Y}})} \|P_{\mathcal{Y}} x - b\|_2^2, \\ \text{s.t.} \quad & MP_{\mathcal{Y}} x = Mb, \end{aligned} \tag{7}$$

where the inner maximization accounts for uncertainty in the system's finite-horizon behavior. Confidence radii ρ with finite-sample guarantees can be derived from subspace-tracking algorithms (Sasfi et al., 2024).

Directly enforcing the constraint in (7) leads to a projected min–max problem on the Grassmannian, which is prohibitively expensive for online control. To obtain a tractable surrogate, we relax the constraint via Tikhonov regularization (Golub et al., 1999), leading to the optimization problem

$$\min_{x \in \mathbb{R}^{qL}} \max_{\mathcal{Y} \in \mathbb{B}_{\rho}^d(\hat{\mathcal{Y}})} \|P_{\mathcal{Y}} x - b\|_2^2 + \gamma \|MP_{\mathcal{Y}} x - Mb\|_2^2, \tag{8}$$

where $\gamma > 0$ penalizes inconsistency with past data. For sufficiently large γ (see exact penalty methods in (Liu and Boumal, 2019)), solutions of (8) approximate those of (7).

Main results

We now present the solution methodology to the problem (8). The following results show that the inner problem has an explicit solution to \mathcal{Y} due to our choice of the chordal distance for the ball constraint.

Lemma 3 *Consider the robust least-squares problem (8). Let $\hat{Y} \in \mathbb{R}^{n \times k}$ and $\hat{\mathcal{Y}} \in \text{Gr}(k, n)$ be given such that $P_{\hat{\mathcal{Y}}} = \pi(\hat{Y})$. Define $f : \mathbb{R}^n \times \text{Gr}(k, n) \rightarrow \mathbb{R}_{\geq 0}$ as*

$$f(x, \mathcal{Y}) := \|P_{\mathcal{Y}}x - b\|_2^2 + \gamma \|MP_{\mathcal{Y}}x - Mb\|_2^2. \quad (9)$$

Then the following hold.

1. *$f(x, \mathcal{Y}^*(x))$ is convex in x , where $\mathcal{Y}^*(x) = \arg \max_{\mathcal{Y} \in \mathbb{B}_\rho^d(\hat{\mathcal{Y}})} f(x, \mathcal{Y})$.*
2. *The gradient of f with respect to x is given by*

$$\nabla_x f(x, \mathcal{Y}^*(x)) = 2P_{\mathcal{Y}^*(x)}(x - b) + 2\gamma P_{\mathcal{Y}^*(x)}M^\top M(P_{\mathcal{Y}^*(x)}x - b). \quad (10)$$

Proof Refer to Supplementary for a detailed proof. ■

Among the available Grassmannian distance metrics—chordal, gap, and related variants—the key consideration is tractability, i.e., whether the inner problem in \mathcal{Y} admits a closed-form solution, as established in the following result. Anticipating the structure of the cost function in (11), we adopt the chordal metric d defined in (2) whose trace representation leads to an explicit and efficient formulation. However, other metrics may also yield tractable variants of the problem and represent a promising direction for future investigation.

Theorem 4 *Consider the robust least-squares problem (8). Let*

$$\mathcal{Y}^*(x) = \arg \max_{\mathcal{Y} \in \mathbb{B}_\rho^d(\hat{\mathcal{Y}})} f(x, \mathcal{Y}),$$

where f is defined in (9) and $Y^ \in \text{St}(k, n)$ such that $\pi(Y^*(x)) = P_{\mathcal{Y}^*(x)}$. Then, there exists $\lambda^* \geq 0$ such that the maximizer $\mathcal{Y}^*(x)$ of the inner problem satisfies the first-order optimality conditions, and*

$$P_{\mathcal{Y}^*(x)} = \pi(Y^*(x)), \quad Y^*(x) = \{\text{top-}k \text{ eigenvectors of } B(x, \lambda^*; \gamma)\},$$

where $B(x, \lambda^; \gamma) = xx^\top - xb^\top - bx^\top + \lambda^*\hat{Y}\hat{Y}^\top + \gamma(xx^\top - M^\top Mb x^\top - xb^\top M^\top M)$.*

Proof The proof proceeds by reformulating the inner maximization into a sequence of equivalent problems, the last of which admits an explicit analytic solution. It can be shown that the inner problem in (8) can be equivalently expressed as

$$\max_{Y \in \text{St}(k, n)} \text{Tr} \left(Y^\top B(x, \lambda; \gamma) Y \right), \quad (11)$$

where $B(x, \lambda; \gamma) := A(x; \gamma) + \lambda \hat{Y} \hat{Y}^\top$ for a particular $\lambda \geq 0$ such that $A(x; \gamma) := xx^\top - xb^\top - bx^\top + \gamma(xx^\top - M^\top Mb x^\top - xb^\top M^\top M)$. The problem (11) has a well-known closed-form solution given by:

$$Y^*(x) = \{\text{top-}k \text{ eigenvectors of } B(x, \lambda^*; \gamma)\}.$$

The corresponding optimal subspace $\mathcal{Y}^*(x)$ is such that $P_{\mathcal{Y}^*(x)} = \pi(Y^*(x))$. The detailed proof is in the Supplementary. \blacksquare

Remark 5 (Characterization of λ^*) *From (Liu and Boumal, 2019, Def. 2.3), for $g(\mathcal{Y}) = d^2(\mathcal{Y}, \hat{\mathcal{Y}}) - \rho^2 \leq 0$ being the inequality constraint, we have complementary slackness for λ^* , such that it satisfies $\lambda^* g(\mathcal{Y}^*) = 0$. Thus, if $\lambda^* = 0$, the the constraint $g(\mathcal{Y}^*) < 0$ must be satisfied, but if $\lambda^* > 0$, then $g(\mathcal{Y}^*) = 0$, i.e., the optimal subspace \mathcal{Y}^* must lie on the boundary of the ball $\mathbb{B}_\rho^d(\hat{\mathcal{Y}})$.*

The above remark implies that if the optimal subspace \mathcal{Y}^* is such that $g(\mathcal{Y}^*) > 0$, then λ^* must be larger so that \mathcal{Y}^* lies on the boundary of the uncertainty ball (worst-case scenario). Analyzing the matrix $B(x, \lambda) = A(x) + \lambda \hat{Y} \hat{Y}^\top$, we observe that since $Y^*(x)$ is the top- k eigenspace of $B(x, \lambda^*)$, increasing λ implies that $\mathcal{Y}^*(x)$ gets closer to $\hat{\mathcal{Y}}$, in the sense that $\mathcal{Y}^*(x)$ depends implicitly on λ , and the optimal subspace is such that $d(\mathcal{Y}^*(x, \lambda^*), \hat{\mathcal{Y}}) = \rho$. Geometrically, lower data uncertainty corresponds to a smaller radius ρ and, consequently, a larger multiplier λ^* , which constrains $\mathcal{Y}^*(x, \lambda^*)$ to remain close to $\hat{\mathcal{Y}}$.

Exploiting the explicit solution proposed to the inner problem in the above results, the min-max optimization simplifies to a convex minimization framework, which can be easily solved with standard methods, such as gradient-based schemes. For example, at each step i , one may compute the gradient $\nabla_x f(x_i, \mathcal{Y}^*(x_i))$ using (10), where $\mathcal{Y}^*(x_i)$ has an explicit solution given in Theorem 4. Thus, we propose the optimization scheme in Algorithm 1 for solving the robust least-squares problem, implemented via standard gradient descent scheme. The convergence of gradient descent is well-established in optimization literature (Nocedal and Wright, 2006, Chapter 3). The gradient $\nabla_x f(x, \mathcal{Y}^*(x))$ can be shown be Lipschitz continuous with Lipschitz constant $L_f = 2 + 2\gamma$, which provides a guarantee for convergence. Standard optimization theory states that Algorithm 1 converges (i.e., $\|\nabla_x f(x, \mathcal{Y}^*(x))\| \leq \text{tolx}$ for some sufficiently small tolerance $\text{tolx} > 0$) to a minimizer x^* for any fixed step-size α , satisfying $0 < \alpha < 2/L_f$, which simplifies to $0 < \alpha < \frac{1}{1+\gamma}$ in our case. Since this minimizer x^* may not be unique (although $P_{\mathcal{Y}^*} x^*$ would be), we could force convergence to a unique minimizer with a norm regularization term $\mu \|x\|^2$, for some small $\mu > 0$.

The subspace optimization problem presented in this section directly connects to the linear quadratic tracking objective described in Section 2.2. In line with the model predictive control (MPC) paradigm, Algorithm 1 is solved at each time step k in a receding-horizon fashion. From the resulting optimal trajectory $w^* = P_{\mathcal{Y}^*} x^* = \text{col}(w_{\text{ini}}^*, w_{\text{f}}^*)$, the first control input of w_{f}^* is extracted and applied to the system, and this is repeated for all $t \in [1, T]$.

4. Numerical Simulations

We present numerical results for the proposed algorithm applied to the finite-horizon linear quadratic tracking problem introduced in Section 2.2. We consider both tracking and regulation tasks in two case studies. In each case, the system dynamics are described by an LTI state-space model

$$x(t+1) = Ax(t) + Bu(t), \quad y(t) = Cx(t) + Du(t) + e(t), \quad (12)$$

Algorithm 1: Proposed Constrained Robust Least-Squares Optimization Algorithm

Data: Subspace Estimate $\hat{Y} \in \mathbb{R}^{n \times k}$, Reference $b \in \mathbb{R}^n$, Cost f .
Input: Initial guess $x_0 \in \mathbb{R}^n$, step-size $\alpha > 0$, $\rho, \gamma > 0$, $\text{tolx} > 0$, $M \in \mathbb{R}^{l \times n}$.
Output: Optimal subspace Y^* , Optimal point x^* .

```

for  $i = 0, 1, 2, \dots$ , do
     $A_i = x_i x_i^\top - x_i b^\top - b x_i^\top + \gamma(x x^\top - M^\top M b x^\top - x b^\top M^\top M)$  ;
     $Y^* = \text{eigs}(A_i, k)$ ;
    if  $d(Y^*, \hat{Y}) \leq \rho$  then
         $\lambda_i^* = 0$ ;
    else
        Find  $\lambda_i^* > 0$  such that  $|d(\text{eigs}(A_i + \lambda_i^* \hat{Y} \hat{Y}^\top, k), \hat{Y}) - \rho| = 0$ ;
         $B_i = A_i + \lambda_i^* \hat{Y} \hat{Y}^\top$ ;
         $Y^* = \text{eigs}(B_i, k)$ ;
    end
     $v_i = \nabla_x f(x_i, \pi(Y^*(x_i)))$ ;
    if  $\|v_i\| \leq \text{tolx}$  then
         $x^* = x_i$ ;
        break;
    else
         $x_{i+1} = x_i - \alpha v_i$ ;
    end
end

```

where $u(t) \in \mathbb{R}^m$ is the input, $y(t) \in \mathbb{R}^p$ is the output, and $x(t) \in \mathbb{R}^n$ is the state, and $e(t) \in \mathbb{R}^p$ is the measurement noise, at time $t \in \mathbb{N}$. We compare the performance of the proposed algorithm with (a) a nominal (non-robust ($\rho = 0$) and noiseless) controller (6) assuming a nominal \hat{Y} , and then with (b) a robust data-driven MPC (DD-MPC) from (Berberich et al., 2021). A key difference is that in our methodology, ρ provides a system-theoretic interpretation as the behavioral subspace uncertainty (Padoan et al., 2022) introduced via noisy trajectories, making it intuitive to estimate ρ . In contrast, the slack variables in the DD-MPC algorithm presented in (Berberich et al., 2021) carry no such interpretation and serve merely as design parameters tuned to noise levels. The codes and utilities to reproduce the experiments are available at <https://github.com/shreyasnb/Robust-least-squares-for-data-driven-control>.

4.1. Double integrator

Consider the system (12) with $A = \begin{bmatrix} 1 & 0.5 \\ 0 & 1 \end{bmatrix}$, $B = \begin{bmatrix} 0.125 \\ 0.5 \end{bmatrix}$, $C = [1 \ 0]$, $D = 0$. The reference to track is $w_{\text{ref}}(t) = \text{col}(0, 1)$. Figure 1 shows the tracking in the presence of measurement noise with noise-to-signal ratio $\sigma = 0.1, 0.2$ in offline subspace identification of \hat{Y} (using Lemmas 1,2), as well as in online control. The tracking performance of the proposed method is consistent in both cases for $\gamma \geq 4$, although very large values are undesirable since they have a negative impact on the optimization performance. For $\gamma < 4$, the constraint in (7) is not implemented correctly, resulting

in inaccurate tracking. It is also crucial to note that similar tracking performance is observed in $\sigma = 0.1$ case, for ball radius $\rho \in (0, \sin(2.5^\circ)]$, beyond which we observe significant (bounded) oscillations around the reference $r = 1$, instead of asymptotic convergence as in Figure 1. Similarly, for $\sigma = 0.2$, we have $\rho \in (0, \sin(4^\circ)]$. The bounds on ρ implies that given a noise level σ , an optimal design choice for ρ exists, which yields the best (asymptotic) tracking performance.

We observe similar tracking performance between the proposed algorithm and DD-MPC for $L = 35$, subspaces in $\text{Gr}(37, 70)$, and other design parameters (see Supplementary). Upon increasing the noise level from $\sigma = 0.1$ to 0.2, we relax our uncertainty radius from $\rho = \sin(1^\circ)$ to $\sin(2^\circ)$, while the slack variable $\lambda_\alpha \bar{\epsilon}$ from (Berberich et al., 2021) would need to be increased from 0.2 to 0.5 to observe similar controller performance (keeping all other parameters constant).

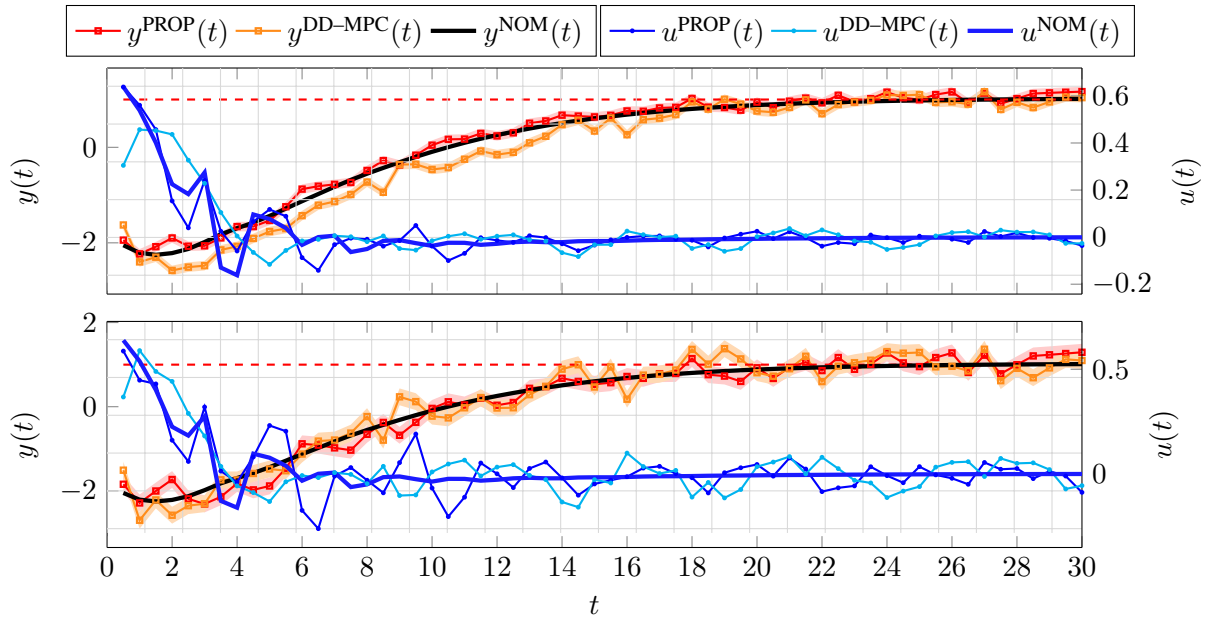


Figure 1: Performance comparison of proposed method (PROP) with DD-MPC and a nominal controller (NOM), of linear quadratic tracking for double-integrator system with reference $r = 1$ (red dashed horizontal line). The first figure shows the trajectories for measurement noise level $\sigma = 0.1$, and the bottom figure is for noise level $\sigma = 0.2$.

4.2. Laplacian system

We consider the system (12) proposed in (Dean et al., 2017, Section 6) with

$$A = \begin{bmatrix} 1.01 & 0.01 & 0 \\ 0.01 & 1.01 & 0.01 \\ 0 & 0.01 & 1.01 \end{bmatrix}, B = I_3, C = [1 \ 0 \ 0], D = 0_{3 \times 1},$$

which corresponds to a discrete-time, marginally unstable Laplacian system. The reference to track is $w_{\text{ref}}(t) = \text{col}(0, 0)$, which is a regulation problem. Figure 2 shows regulation with varying levels ($\sigma = 0.1, 0.2$) of measurement noise, comparing our proposed method with DD-MPC and the nominal regulator (6). It is observed that for $\gamma \geq 1.2$, the regulation performance is consistent in both

noise cases. For the $\sigma = 0.1$ case, similar performance is observed for ball radius $\rho \in (0, \sin(5^\circ)]$, beyond which we see significant drifting around the reference, without the asymptotic behavior. Increasing the noise level to $\sigma = 0.2$, we note that the same trend holds for $\rho \in (0, \sin(6.5^\circ)]$.

Regulation performance is similar for $\sigma = 0.1$ between the proposed algorithm, nominal controller and DD-MPC for $L = 35$, subspaces in $\text{Gr}(108, 140)$, and other parameters (see Supplementary). For $\sigma = 0.2$ however, we observe slightly better regulation for the proposed algorithm compared to DD-MPC. The ball radius was updated from $\rho = \sin(2^\circ)$ to $\sin(3.5^\circ)$ due to the increase in noise level, while the slack variable $\lambda_\alpha \bar{\epsilon}$ from (Berberich et al., 2021) had to be increased from 0.1 to 5 for minimal drifting, to observe the regulation performance shown in Fig. 2.

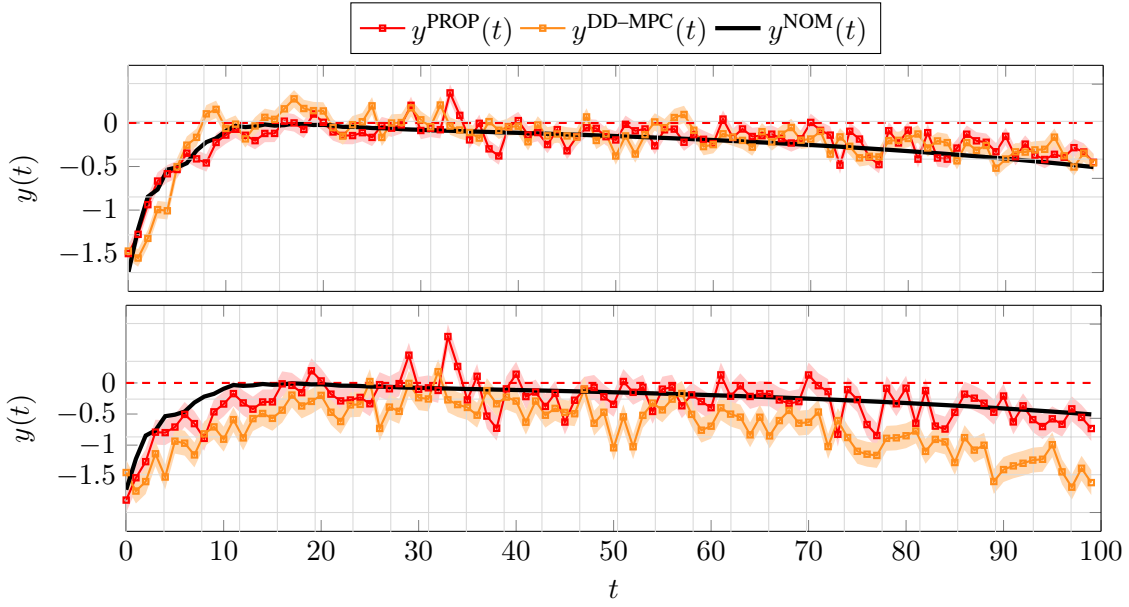


Figure 2: Performance comparison of proposed method (PROP) with DD-MPC, for linear quadratic tracking of the Laplacian system in Section 4.2 with reference $r = 0$. The first figure shows the tracking for measurement noise level $\sigma = 0.1$, and the bottom figure is for noise level $\sigma = 0.2$.

5. Conclusion

This work extended a geometrically grounded framework for least-squares to robust data-driven predictive control. By modeling behavioral subspace uncertainty as a metric ball on the Grassmannian manifold, we obtained a tractable min–max formulation. The core contribution is a closed-form solution to the inner maximization problem, leading to an efficient convex optimization algorithm. The resulting method enhances robustness in data-enabled predictive control, offering clear geometric interpretation and favorable computational scaling. The framework’s generality and efficiency make it promising for extensions to broader classes of data-driven estimation and control problems.

References

P.-A. Absil, R. Mahony, and R. Sepulchre. *Optimization Algorithms on Matrix Manifolds*. Princeton University Press, USA, 2007. ISBN 0691132984.

Brian D. O. Anderson and John B. Moore. *Optimal control: linear quadratic methods*. Prentice-Hall, Inc., USA, 1990. ISBN 0136385605.

J. Berberich, J. Köhler, M. A. Müller, and F. Allgöwer. Linear tracking mpc for nonlinear systems—part II: The data-driven case. *IEEE Transactions on Automatic Control*, 67(9):4406–4421, 2022.

Julian Berberich, Johannes Köhler, Matthias A. Müller, and Frank Allgöwer. Data-driven model predictive control with stability and robustness guarantees. *IEEE Transactions on Automatic Control*, 66(4):1702–1717, 2021. doi: 10.1109/TAC.2020.3000182.

D. Bertsekas. *Nonlinear Programming*. Athena scientific optimization and computation series. Athena Scientific, 2016. ISBN 9781886529052.

Nicolas Boumal. *An introduction to optimization on smooth manifolds*. Cambridge University Press, 2023. doi: 10.1017/9781009166164. URL <https://www.nicolasboumal.net/book>.

Stephen Boyd and Lieven Vandenberghe. *Convex Optimization*. Cambridge University Press, 2004.

V. Breschi, A. Chiuso, and S. Formentin. Data-driven predictive control in a stochastic setting: a unified framework. *Automatica*, 152:110961, 2023.

J. Coulson, A. Padoan, and C. Mostajeran. Geometrically robust least squares through manifold optimization. In *Proc. 26th Int. Symp. Math. Theory of Networks and Systems (MTNS)*, Cambridge, UK, 2025.

Jeremy Coulson, John Lygeros, and Florian Dörfler. Data-enabled predictive control: In the shallows of the deepc. In *2019 18th European Control Conference (ECC)*, pages 307–312, 2019. doi: 10.23919/ECC.2019.8795639.

C. De Persis and P. Tesi. Formulas for data-driven control: Stabilization, optimality, and robustness. *IEEE Transactions on Automatic Control*, 65(3):909–924, 2019.

Sarah Dean, Horia Mania, Nikolai Matni, Benjamin Recht, and Stephen Tu. On the sample complexity of the linear quadratic regulator. *Foundations of Computational Mathematics*, 20, 10 2017. doi: 10.1007/s10208-019-09426-y.

Jean-Pierre Delmas. Subspace tracking for signal processing. In *Adaptive signal processing : next generation solutions*, pages 211 – 270. Wiley-IEEE Press, 2010. URL <https://hal.science/hal-01320647>.

Florian Dörfler, Jeremy Coulson, and Ivan Markovsky. Bridging direct and indirect data-driven control formulations via regularizations and relaxations. *IEEE Transactions on Automatic Control*, 68(2):883–897, 2023. doi: 10.1109/TAC.2022.3148374.

Laurent El Ghaoui and Hervé Lebret. Robust solutions to least-squares problems with uncertain data. *SIAM Journal on Matrix Analysis and Applications*, 18(4):1035–1064, 1997. doi: 10.1137/S0895479896298130. URL <https://doi.org/10.1137/S0895479896298130>.

Carl Friedrich Gauss. *Theoria motus corporum coelestium in sectionibus conicis solem ambientum*. F. Perthes and I.H. Besser, Hamburg, 1809. URL https://archive.org/details/bub_gb_ORUOAAAAQAAJ.

Gene H. Golub and Charles F. Van Loan. An analysis of the total least squares problem. *SIAM Journal on Numerical Analysis*, 17(6):883–893, 1980. doi: 10.1137/0717073.

Gene H. Golub and Charles F. Van Loan. *Matrix Computations - 4th Edition*. Johns Hopkins University Press, Philadelphia, PA, 2013. doi: 10.1137/1.9781421407944. URL <https://epubs.siam.org/doi/abs/10.1137/1.9781421407944>.

Gene H. Golub, Per Christian Hansen, and Dianne P. O’Leary. Tikhonov regularization and total least squares. *SIAM Journal on Matrix Analysis and Applications*, 21(1):185–194, 1999. doi: 10.1137/S0895479897326432. URL <https://doi.org/10.1137/S0895479897326432>.

Jun He, Laura Balzano, and Arthur Szlam. Incremental gradient on the grassmannian for on-line foreground and background separation in subsampled video. *2012 IEEE Conference on Computer Vision and Pattern Recognition*, pages 1568–1575, 2012. URL <https://api.semanticscholar.org/CorpusID:17060463>.

Linbin Huang, Jianzhe Zhen, John Lygeros, and Florian Dörfler. Robust data-enabled predictive control: Tractable formulations and performance guarantees, 2021. URL <https://arxiv.org/abs/2105.07199>.

Changshuo Liu and Nicolas Boumal. Simple algorithms for optimization on riemannian manifolds with constraints, 2019. URL <https://arxiv.org/abs/1901.10000>.

I. Markovsky and F. Dörfler. Behavioral systems theory in data-driven analysis, signal processing, and control. *Annual Reviews in Control*, 52:42–64, 2021. doi: 10.1016/j.arcontrol.2021.09.005.

I. Markovsky and F. Dörfler. Identifiability in the behavioral setting. *IEEE Trans. Automat. Contr.*, 68:1667–1677, 2023. doi: 10.1109/TAC.2022.3209954.

I. Markovsky and P. Rapisarda. Data-driven simulation and control. *Int. J. Contr.*, 81(12):1946–1959, 2008. doi: 10.1080/00207170801942170.

Ivan Markovsky and Sabine Van Huffel. Overview of total least-squares methods. *Signal Processing*, 87(10):2283–2302, 2007. ISSN 0165-1684. doi: <https://doi.org/10.1016/j.sigpro.2007.04.004>. Special Section: Total Least Squares and Errors-in-Variables Modeling.

D.Q. Mayne, M.M. Seron, and S.V. Raković. Robust model predictive control of constrained linear systems with bounded disturbances. *Automatica*, 41(2):219–224, 2005. ISSN 0005-1098. doi: <https://doi.org/10.1016/j.automatica.2004.08.019>. URL <https://www.sciencedirect.com/science/article/pii/S0005109804002870>.

Jorge Nocedal and Stephen J. Wright. *Numerical Optimization*. Springer Series in Operations Research and Financial Engineering. Springer, New York, NY, second edition, 2006.

A. Padoan and J. Coulson. Distances between finite-horizon linear behaviors. *IEEE Control Systems Letters*, 9:1772–1777, 2025. doi: 10.1109/LCSYS.2025.3576312.

Alberto Padoan, Jeremy Coulson, Henk J. Van Waarde, John Lygeros, and Florian Dorfler. Behavioral uncertainty quantification for data-driven control. In *2022 IEEE 61st Conference on Decision and Control, CDC 2022*, Proceedings of the IEEE Conference on Decision and Control, pages 4726–4731. IEEE, 2022. ISBN 978-1-6654-6762-9. doi: 10.1109/CDC51059.2022.9993002.

András Sasfi, Alberto Padoan, Ivan Markovsky, and Florian Dörfler. Subspace tracking for online system identification, 2024. URL <https://arxiv.org/abs/2412.09052>.

P.O.M. Scokaert and D.Q. Mayne. Min-max feedback model predictive control for constrained linear systems. *IEEE Transactions on Automatic Control*, 43(8):1136–1142, 1998. doi: 10.1109/9.704989.

Jan C. Willems. From time series to linear system—part i. finite dimensional linear time invariant systems. *Automatica*, 22(5):561–580, 1986. ISSN 0005-1098. doi: [https://doi.org/10.1016/0005-1098\(86\)90066-X](https://doi.org/10.1016/0005-1098(86)90066-X).

JC Willems, P Rapisarda, Markovsky, and BLM De Moor. A note on persistency of excitation. *Systems & Control Letters*, 54(4):325–329, April 2005. ISSN 0167-6911. doi: 10.1016/j.sysconle.2004.09.003.

Yifan Xie, Julian Berberich, Felix Brändle, and Frank Allgöwer. Data-driven min-max mpc for lpv systems with unknown scheduling signal, 2024. URL <https://arxiv.org/abs/2411.05624>.

Yifan Xie, Julian Berberich, Robin Strässer, and Frank Allgöwer. Bilinear data-driven min-max mpc: Designing rational controllers via sum-of-squares optimization, 2025. URL <https://arxiv.org/abs/2504.04870>.

Yifan Xie, Julian Berberich, and Frank Allgöwer. Data-driven min–max mpc for linear systems: Robustness and adaptation. *Automatica*, 183:112612, 2026. ISSN 0005-1098. doi: <https://doi.org/10.1016/j.automatica.2025.112612>. URL <https://www.sciencedirect.com/science/article/pii/S0005109825005072>.

Supplementary Sections

Appendix A. Detailed Preliminaries

Grassmann Manifold Geometry

The *Grassmannian* $\text{Gr}(k, n)$ is the Riemannian manifold of all k -dimensional linear subspaces of \mathbb{R}^n (Boumal, 2023). A standard way to describe it is through the *Stiefel manifold*

$$\text{St}(k, n) := \{ Y \in \mathbb{R}^{n \times k} : Y^\top Y = I_k \}, \quad (13)$$

whose elements are matrices with orthonormal columns. The orthonormality constraints $Y^\top Y = I_k$ define a smooth surface in $\mathbb{R}^{n \times k}$, so $\text{St}(k, n)$ is a smooth manifold of dimension $nk - \frac{k(k+1)}{2}$ (Boumal, 2023). Different matrices in $\text{St}(k, n)$ may span the same subspace, and identifying all orthonormal bases that generate the same subspace yields a smooth manifold structure. Equivalently, the Grassmannian can be viewed as the space of equivalence classes of $\text{St}(k, n)$ under right multiplication by elements of $O(k)$, the group of all $k \times k$ orthogonal matrices.

An alternative and particularly convenient representation uses orthogonal projection matrices. Every k -dimensional subspace \mathcal{Y} of \mathbb{R}^n admits a unique orthogonal projector $P_{\mathcal{Y}}$, which makes this identification natural. In this representation, the Grassmannian can be written as

$$\text{Gr}(k, n) = \{ P \in \mathbb{R}^{n \times n} : P^\top = P, P^2 = P, \text{rank}(P) = k \},$$

so that each point corresponds to a unique symmetric, idempotent matrix of rank k , and the associated k -dimensional subspace is given by the image of P .

The link between these two representations is given by the canonical projection

$$\pi : \text{St}(k, n) \rightarrow \text{Gr}(k, n), \quad \pi(Y) = YY^\top,$$

which maps an orthonormal basis Y to the orthogonal projector onto its span. The map π identifies all bases spanning the same subspace, since YQ and Y yield the same projector for any $Q \in O(k)$. Equivalently, π is constant along right- $O(k)$ orbits, that is, sets of the form $\{YQ : Q \in O(k)\}$, and thus becomes injective on the quotient $\text{St}(k, n)/O(k)$.

The Grassmannian admits a natural smooth Riemannian structure, inherited from the canonical quotient metric on $\text{St}(k, n)/O(k)$. For any $\mathcal{Y} \in \text{Gr}(k, n)$ represented by $Y \in \text{St}(k, n)$, the tangent space is

$$T_{\mathcal{Y}}\text{Gr}(k, n) = \{ V \in \mathbb{R}^{n \times k} \mid Y^\top V = 0 \}.$$

where tangent directions are matrices orthogonal (column-wise) to Y , reflecting that motion on the manifold preserves the orthonormality constraint (Boumal, 2023).

Given a smooth function $f : \text{Gr}(k, n) \rightarrow \mathbb{R}$, its Riemannian gradient at \mathcal{Y} is obtained by projecting the Euclidean gradient of any smooth extension $\bar{f} : \mathbb{R}^{n \times k} \rightarrow \mathbb{R}$ onto the tangent space:

$$\text{grad}f(\mathcal{Y}) = P_{\mathcal{Y}}^\perp \nabla \bar{f}(Y), \quad P_{\mathcal{Y}}^\perp := I_n - YY^\top,$$

where \bar{f} satisfies $\bar{f}(Y) = f(\mathcal{Y})$ for any orthonormal basis Y of \mathcal{Y} , and $\nabla \bar{f}(Y)$ denotes the standard Euclidean gradient of \bar{f} .

Several distances can be used to compare subspaces (Boumal, 2023), such as geodesic, projection, and Procrustes distances. The *chordal distance* is particularly convenient because it admits a simple expression in terms of projection matrices and is computationally efficient. It is defined as

$$d_2(\mathcal{Y}_1, \mathcal{Y}_2) := \sqrt{\text{Tr}\left(P_{\mathcal{Y}_1}^{\perp} P_{\mathcal{Y}_2}\right)},$$

and measures the discrepancy between the projectors. The chordal distance is invariant under changes of orthonormal bases and depends only on the principal angles between the subspaces, capturing how much one subspace deviates from the other.

The chordal metric is closely related to the *gap metric* (Boumal, 2023), defined as

$$d_{\infty}(\mathcal{Y}_1, \mathcal{Y}_2) := \|P_{\mathcal{Y}_1} - P_{\mathcal{Y}_2}\|_2,$$

which measures the largest principal angle between the subspaces. The two metrics are equivalent (see Padoan et al. (2022) and references therein) on $\text{Gr}(k, n)$, and satisfy

$$d_{\infty}(\mathcal{Y}_1, \mathcal{Y}_2) \leq d_2(\mathcal{Y}_1, \mathcal{Y}_2) \leq \sqrt{k} d_{\infty}(\mathcal{Y}_1, \mathcal{Y}_2),$$

so the gap distance controls the worst-case angular deviation, whereas the chordal distance aggregates the contribution of all principal angles. When average or aggregate separation is more informative than the largest principal angle, the chordal metric provides a natural and tractable choice.

Appendix B. Proof of Lemma 3

Proof Fix $\mathcal{Y} \in \mathbb{B}_{\rho}^d(\hat{\mathcal{Y}})$. Then $P_{\mathcal{Y}}$ is a constant symmetric idempotent matrix ($P_{\mathcal{Y}} = P_{\mathcal{Y}}^{\top} = P_{\mathcal{Y}}^2$). Defining $r(x) := P_{\mathcal{Y}}x - b$, we have

$$\begin{aligned} f(x, \mathcal{Y}) &= \|r(x)\|_2^2 + \gamma \|Mr(x)\|_2^2 \\ &= x^{\top} P_{\mathcal{Y}}x - 2b^{\top} P_{\mathcal{Y}}x + \|b\|_2^2 + \gamma x^{\top} P_{\mathcal{Y}}M^{\top}MP_{\mathcal{Y}}x - 2\gamma b^{\top} M^{\top}MP_{\mathcal{Y}}x + \gamma \|Mb\|_2^2. \end{aligned}$$

Since $P_{\mathcal{Y}} \succeq 0$ and $P_{\mathcal{Y}}M^{\top}MP_{\mathcal{Y}} \succeq 0$, $f(\cdot, \mathcal{Y})$ is a convex quadratic in x . Therefore $g(x) = \sup_{\mathcal{Y} \in \mathbb{B}_{\rho}^d(\hat{\mathcal{Y}})} f(x, \mathcal{Y})$ is the pointwise supremum of convex functions and is convex (Boyd and Vandenberghe, 2004, Sec. 3.2.3).

For the gradient, f is continuously differentiable in x for each \mathcal{Y} , and $\mathbb{B}_{\rho}^d(\hat{\mathcal{Y}})$ is compact in $\text{Gr}(k, n)$; therefore, Danskin's theorem applies (e.g. (Bertsekas, 2016, Prop. B.22)). If the maximizer is unique,

$$\nabla g(x) = \nabla_x f(x, \mathcal{Y}^*(x)).$$

Differentiating (9) in x (with $P_{\mathcal{Y}}$ treated as constant) and using $P_{\mathcal{Y}} = P_{\mathcal{Y}}^{\top}$ yields

$$\nabla_x f(x, \mathcal{Y}) = 2P_{\mathcal{Y}}(P_{\mathcal{Y}}x - b) + 2\gamma P_{\mathcal{Y}}M^{\top}M(P_{\mathcal{Y}}x - b),$$

which gives (10) after substituting $\mathcal{Y} = \mathcal{Y}^*(x)$. If the maximizer is not unique, Danskin's theorem further yields the stated subgradient characterization. \blacksquare

Appendix C. Proof of Theorem 4

Proof The proof proceeds by reformulating the inner maximization into a sequence of equivalent problems, the last of which admits an explicit analytic solution. First, inner problem in (8) can be simplified using the identity $\langle v_1, v_2 \rangle = \text{Tr}(v_1 v_2^\top)$ for all $v_1, v_2 \in \mathbb{R}^n$, where $\langle \cdot, \cdot \rangle$ is the standard inner product in Euclidean space. Using $P = P^2$, $MM^\top = I_l$ and ignoring constants which do not affect the optimizer, the inner problem in (8) can be equivalently expressed as

$$\max_{\mathcal{Y} \in \mathbb{B}_\rho^d(\hat{\mathcal{Y}})} \langle P_{\mathcal{Y}}x, (x - b) \rangle - \langle P_{\mathcal{Y}}b, x \rangle + \gamma \langle P_{\mathcal{Y}}M^\top MP_{\mathcal{Y}}x, (x - b) \rangle - \gamma \langle P_{\mathcal{Y}}M^\top Mb, x \rangle, \quad \forall x \in \mathbb{R}^n.$$

Defining $A(x; \gamma) := xx^\top - xb^\top - bx^\top + \gamma(xx^\top - M^\top Mb x^\top - xb^\top M^\top M)$, we obtain

$$\max_{\mathcal{Y} \in \mathbb{B}_\rho^d(\hat{\mathcal{Y}})} \text{Tr}(P_{\mathcal{Y}}A(x; \gamma)), \quad \forall x \in \mathbb{R}^n. \quad (14)$$

We define the inequality constraint due to the ball $g(\mathcal{Y}) := d(\mathcal{Y}, \hat{\mathcal{Y}})^2 - \rho^2 \leq 0$. Using the definition of d in (2), we have $g(\mathcal{Y}) = k - \text{Tr}(P_{\mathcal{Y}}P_{\hat{\mathcal{Y}}}) - \rho^2$. The constrained problem (14) can be solved by using an exact penalty function (Liu and Boumal, 2019) :

$$\max_{\mathcal{Y} \in \text{Gr}(k, n)} \text{Tr}(P_{\mathcal{Y}}A(x; \gamma)) - \lambda g(\mathcal{Y}) \quad \forall x \in \mathbb{R}^n$$

for a sufficiently large constraint multiplier $\lambda \in \mathbb{R}_{\geq 0}$, such that the local maximizer \mathcal{Y}^* to the above problem is also the local maximizer of (14). Replacing $P_{\mathcal{Y}} = YY^\top$, $P_{\hat{\mathcal{Y}}} = \hat{Y}\hat{Y}^\top$ produces

$$\max_{Y \in \text{St}(k, n)} \text{Tr}\left(Y^\top \left[A(x; \gamma) + \lambda \hat{Y}\hat{Y}^\top\right] Y\right).$$

Defining $B(x, \lambda; \gamma) := A(x; \gamma) + \lambda \hat{Y}\hat{Y}^\top$, we obtain

$$\max_{Y \in \text{St}(k, n)} \text{Tr}\left(Y^\top B(x, \lambda; \gamma) Y\right). \quad (15)$$

Alternatively, considering the inner problem in (8), we define the Lagrangian function $\mathcal{L}(x, \mathcal{Y}, \lambda) := f(x, \mathcal{Y}) - \lambda g(\mathcal{Y})$, for $\lambda \in \mathbb{R}_{\geq 0}$, such that we equivalently have:

$$\max_{\mathcal{Y} \in \text{Gr}(k, n)} \min_{\lambda} \mathcal{L}(x, \mathcal{Y}, \lambda) = \max_{\mathcal{Y} \in \text{Gr}(k, n)} \min_{\lambda} f(x, \mathcal{Y}) - \lambda g(\mathcal{Y}), \quad \text{for some } x \in \mathbb{R}^n.$$

From first-order optimality conditions (Liu and Boumal, 2019, Def. 2.3), we have

$$\text{grad}_{\mathcal{Y}} \mathcal{L}(x, \mathcal{Y}^*, \lambda^*) = 0 \implies \text{grad}_{\mathcal{Y}} f(x, \mathcal{Y}^*) = \lambda^* \text{grad}_{\mathcal{Y}} g(\mathcal{Y}^*),$$

where \mathcal{Y}^* and λ^* are optimal. Taking the Riemannian gradient (see Section 2), we obtain

$$\begin{aligned} & \left(I - Y^*Y^{*\top}\right) A(x; \gamma) Y^* = \lambda^* \left(I - Y^*Y^{*\top}\right) \hat{Y}\hat{Y}^\top Y^* \\ & \implies B(x, \lambda^*; \gamma) Y^* = Y^* \left[Y^{*\top} B(x, \lambda^*; \gamma) Y^*\right], \end{aligned} \quad (16)$$

where $B(x, \lambda^*; \gamma) = A(x; \gamma) + \lambda^* \hat{Y}\hat{Y}^\top$. The stationary condition in (16) is the well-known eigenvalue problem (Absil et al., 2007, Section 2.1) with the explicit solution

$$Y^*(x) = \{\text{top-k eigenvectors of } B(x, \lambda^*; \gamma)\}.$$

This claim is also supported by the problem structure observed in (15). The corresponding optimal subspace $\mathcal{Y}^*(x)$ is such that $P_{\mathcal{Y}^*(x)} = \pi(Y^*(x))$. ■

Appendix D. Additional Simulations Details

The simulations are performed to show similar performance of our min-max, robust, direct data-driven controller with robust MPC (indirect) data-driven control (Berberich et al., 2021). Both algorithms are implemented in MATLAB, where PROP uses custom code for gradient descent, and DD-MPC uses YALMIP toolbox, available at <https://yalmip.github.io>, to solve the problem as a semi-definite programming problem.

DD-MPC. The DD-MPC algorithm proposes to solve the problem (subject to additional constraints):

$$\begin{aligned} \min_{\alpha(t), \sigma(t), \bar{u}(t), \bar{y}(t)} \quad & \ell(\bar{u}_k(t), \bar{y}_k(t)) + \lambda_\alpha \bar{\epsilon} \|\alpha(t)\|_2^2 + \lambda_\sigma \|\sigma(t)\|_2^2 \\ \text{subject to} \quad & \|\sigma_k(t)\|_\infty \leq \bar{\epsilon}(1 + \|\alpha(t)\|_1) \end{aligned}$$

where

$$\ell(\bar{u}, \bar{u}) = \|\bar{u} - u^s\|_Q^2 + \|\bar{y} - y^s\|_R^2,$$

for $Q, R \succ 0$, (u^s, y^s) is the desired equilibrium, σ is a slack variable to account for noisy measurements (robustness) and $\lambda_\alpha \bar{\epsilon}, \lambda_\sigma > 0$ are regularization weights which depend on the noise level.

Parameters. The parameters for our simulations (PROP) are tabulated below:

Parameter	Value
T_{ini}	10
T_f	25
L	35
n	70
k	37
γ	4
tolx	10^{-6}
α	0.1
T	115

Parameter	Value
T_{ini}	10
T_f	25
L	35
n	140
k	108
γ	4
tolx	10^{-6}
α	0.1
T	150

Table 1: Parameters for double integrator

Table 2: Parameters for Laplacian system.

Parameters for simulations of DD-MPC (Berberich et al., 2021) are also tabulated below:

Parameter	Value
T_{ini}	10
T_f	25
L	35
Q	I_2
R	0.5
λ_σ	10^3
T	115

Parameter	Value
T_{ini}	10
T_f	25
L	35
Q	$0.1I_3$
R	5
λ_σ	10^3
T	150

Table 3: Parameters for double integrator.

Table 4: Parameters for Laplacian system.

Results. The control inputs (PROP) for the Laplacian system corresponding to the outputs shown in Figure 2 are shown below in Figure 3 for completeness. For both case studies, we present the optimization convergence plots for double integrator in Figure 4 and for the Laplacian system in Figure 5, by examining the performance of Algorithm 1 at some time-step during the simulation.

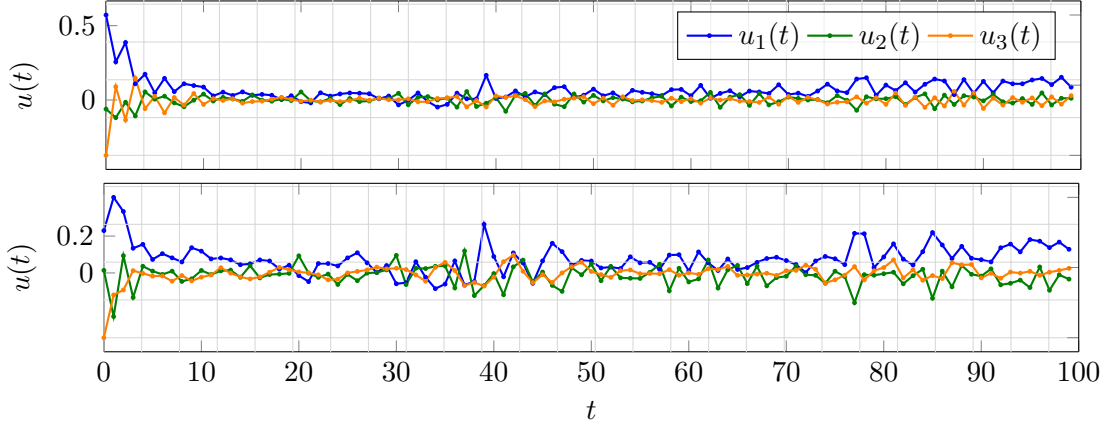


Figure 3: Optimal control inputs for LQR of Laplacian system. The first figure shows the tracking for measurement noise level $\sigma = 0.1$, and the bottom figure is for noise level $\sigma = 0.2$.

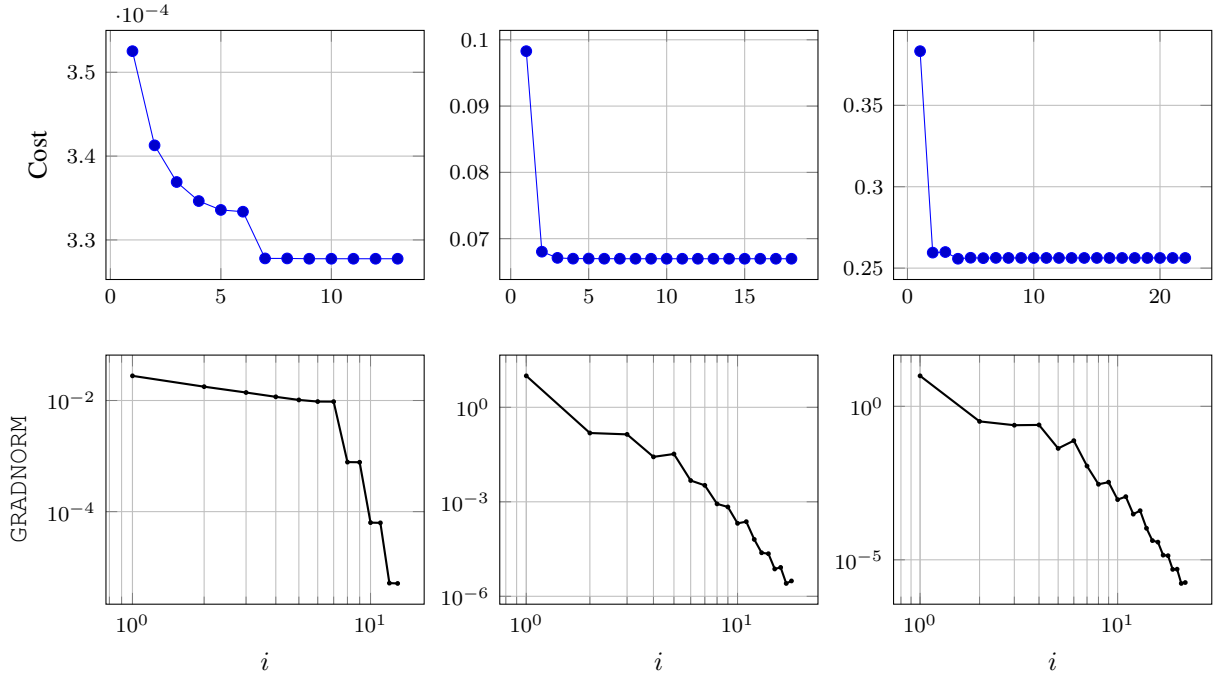


Figure 4: Cost $f(x_i, \mathcal{Y}^*(x_i))$ and gradnorm $\|\nabla_x f(x_i, \mathcal{Y}^*(x_i))\|$ evolution with iteration index i , at $t = 50$: First column corresponds to nominal (NOM) algorithm, second column corresponds to the (PROP) algorithm for $\sigma = 0.1$ and third column is for $\sigma = 0.2$.

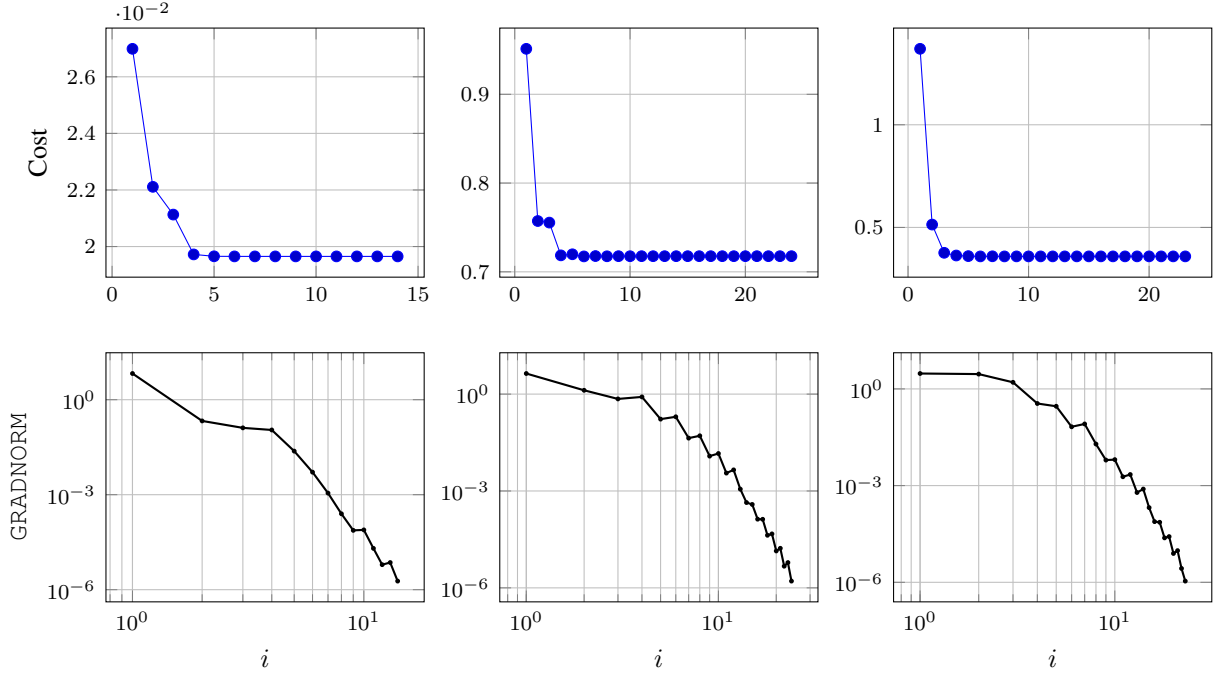


Figure 5: Cost $f(x_i, \mathcal{Y}^*(x_i))$ and gradnorm $\|\nabla_x f(x_i, \mathcal{Y}^*(x_i))\|$ evolution with iteration index i , at $t = 10$: First column corresponds to nominal (NOM) algorithm, second column corresponds to the (PROP) algorithm for $\sigma = 0.1$ and third column is for $\sigma = 0.2$.

Figure 6 shows the evolution of the constraint multiplier λ^* for the double integrator. We observe that as the trajectories asymptotically track the reference, the penalty λ^* decreases (roughly) asymptotically to zero. Similar trends are observed for the Laplacian system as seen in Figure 7.

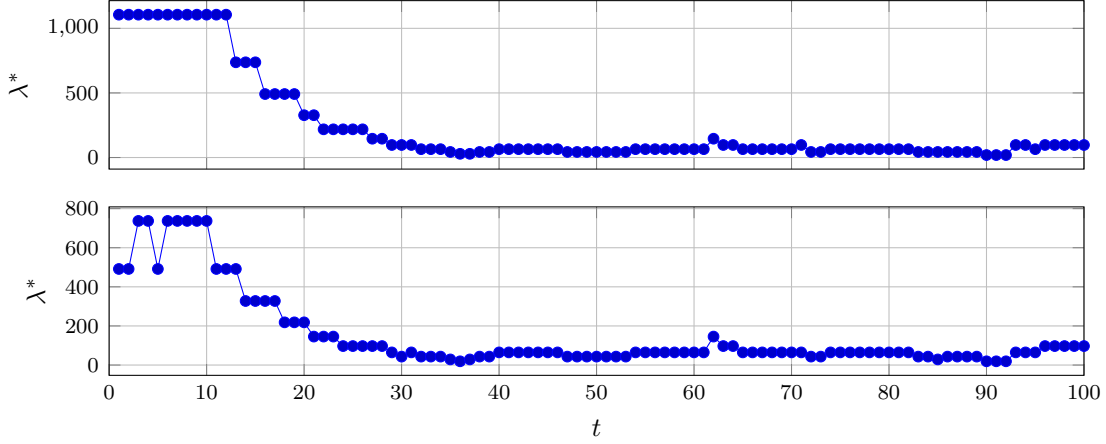


Figure 6: Constraint multiplier λ^* at each time-step of the double-integrator reference tracking. Top and bottom figures corresponding to noise levels $\sigma = 0.1$ and $\sigma = 0.2$ respectively.

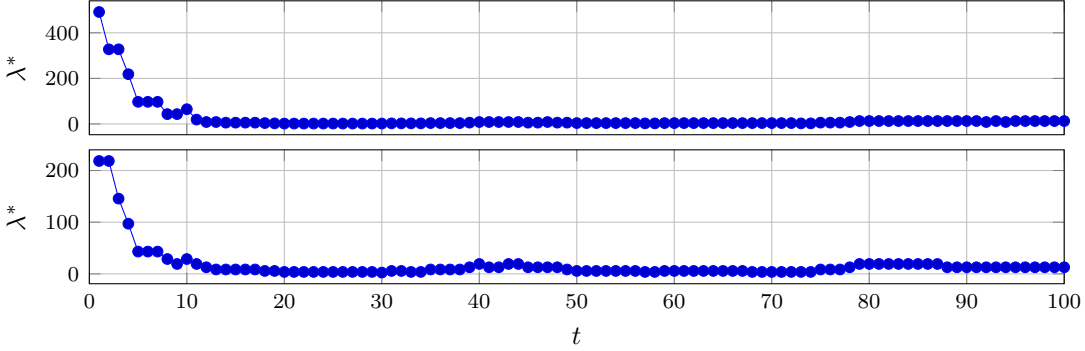


Figure 7: Constraint multiplier λ^* at each time-step of the Laplacian system regulation. Top and bottom figures corresponding to noise levels $\sigma = 0.1$ and $\sigma = 0.2$ respectively.

Comparison with TSRGDA (Coulson et al., 2025)

We compare the convergence performance of our proposed algorithm with (Coulson et al., 2025) which uses timescale-separated Riemannian gradient descent-ascent (TSRGDA) algorithm to solve the robust least-squares problem. Here we only examine the robust least-squares problem (1). Consider subspaces in $\text{Gr}(37, 70)$, $\rho = \sin(\pi/8)$ and $\hat{\mathcal{Y}} = \text{im} \begin{bmatrix} I_{37} \\ 0_{33 \times 37} \end{bmatrix}$. The parameters used for TSRGDA are shown in Table 5.

Parameter	Value
λ	1000
u	0.1
η_x	10^{-4}
η_y	10^{-3}

Table 5: Parameters for TSRGDA.

From Figure 8, we observe that for the TSRGDA algorithm, it takes $\sim 10^5$ iterations for the gradnorm to reach within a tolerance of 10^{-5} whereas the proposed algorithm reaches it within $\sim 10^3$ iterations. It is also crucial to note that for the proposed algorithm, due to the explicit solution of $\mathcal{Y}^*(x_i)$, we observe that $\|\text{grad}_{\mathcal{Y}} f(x_i, \mathcal{Y}^*(x_i))\| \sim 10^{-14}$ for all iterates $i = 0, 1, \dots$. This is the crucial novelty of the proposed algorithm, wherein the min-max setup is elegantly converted to a convex optimization framework. The run time for the proposed method for the gradnorm (w.r.t x) to reach $\text{tol}_x = 10^{-4}$ is 3.2 seconds, whereas the TSRGDA method takes 25 seconds. Increasing the step-sizes η_x, η_y leads to negative effect on convergence. Thus, along with tractability and efficiency, the proposed method also guarantees convergence for $\alpha \in (0, 1]$.

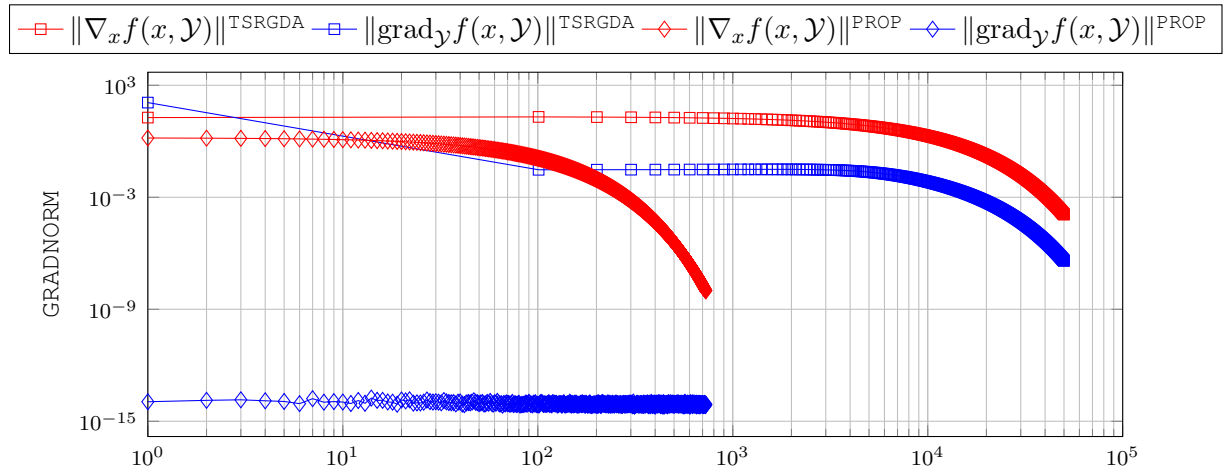


Figure 8: Gradnorm comparison between TSRGDA and proposed method (PROP).